Dalton Transactions

Complete On/Off Responsive ParaCEST MRI Contrast Agents for Copper and Zinc

Journal:	*Dalton Transactions*
Manuscript ID	DT-ART-03-2018-001172.R1
Article Type:	Paper
Date Submitted by the Author:	17-May-2018

Complete List of Authors:	Srivastava, Kriti ; University of Minnesota, Department of Chemistry Ferrauto, Giuseppe; University of Torino, Chemistry IFM Harris, Sarah; University of Minnesota, Department of Chemistry Longo, Dario; University of Torino, Department of Molecular Biotechnologies and Health Sciences Botta, Mauro; Università del Piemonte Orientale, Dipartimento di Scienze e Innovazione Tecnologica Aime, Silvio; University of Torino, Chemistry IFM Pierre, Valerie; University of Minnesota, Department of Chemistry

Complete On/Off Responsive ParaCEST MRI Contrast Agents for Copper and Zinc

Received 00th January 20xx,
Accepted 00th January 20xx

DOI: 10.1039/x0xx00000x

www.rsc.org/

K. Srivastava,[a]† G. Ferrauto,[b]† S. M. Harris,[a] D. L. Longo,[b] M. Botta,[c] S. Aime[b] and V. C. Pierre[a]*

Two thulium-based ParaCEST responsive contrast agents, Tm-DOTAm-py and Tm-DOTAm-βAla-py, have been synthesized and evaluated for imaging copper and zinc. Unusual for responsive MRI contrast agents, both agents display a complete on/off response in the presence of the transition metals. Both complexes function as paraCEST agents in the absence of copper and zinc, with the positively charged Tm-DOTAm-py being more sensitive than the neutrally charged Tm-DOTAm-βAla-py. In each case, the CEST signal arises from the amides' protons rather than from a water molecule coordinated to the Tm^{3+} ion. Upon binding to Cu^{I}, Cu^{II}, or Zn^{II}, the exchange rate of the amide protons increases substantially, resulting in a complete loss of the CEST signal. This efficient mode of action along with the lack of inner-sphere water molecule both in the presence and absence of transition metals was confirmed by $1/T_1$ NMRD profiles, ^{17}O NMR measurements, and molecular modelling simulations. Neither complex is selective for copper over zinc. Both form either a 1:1 TmL:Cu^{+} or a 2:1 TmL:Cu^{2+} and TmL:Zn^{2+} complexes with binding affinities comparable to that of other responsive MRI contrast agents and sensitivity comparable to other CEST contrast agents.

Introduction

Zinc and copper are essential to several biological pathways. Disruption of their homeostasis is implicated in the physiology and pathology of patients suffering from aging or neurodegenerative diseases including Alzheimer's and Parkinson's,[1] as well as Wilson's disease,[2] Menkes syndrome[3] and certain tumors.[4] Zinc ion is involved in the regulation of gene transcription and in multiple cell signaling pathways, particularly in regulating pancreatic function and in apoptosis.[5] Zinc and copper have both been shown to modulate neuronal transmission in the brain;[6] both can contribute to neuronal injury under certain acute conditions and can induce the formation of Aβ amyloid plaques in the brain of patients suffering from Alzheimer's disease.[7] In the latter case, both the intra- and extracellular concentrations of copper and zinc can vary substantially between healthy and diseased patients. For instance, these two transition metals are present in substantially higher concentrations extracellularly in Aβ plaques: up to 0.4 mM of Cu^{2+} and 0.2-1 mM Zn^{2+} are present in Aβ plaques, two and three orders of magnitude higher than in the extracellular environment of a healthy brain.[8-12]

Altogether, the physiological and pathological roles of these metal ions and the large difference in concentration between healthy and diseased tissues makes them good targets for the development of *in vivo* imaging agents. Among the other *in vivo* imaging modalities, magnetic resonance imaging (MRI) is particularly well suited for this purpose because of its non-invasive nature and its ability to produce high-resolution, three-dimensional images of deep tissues without using harmful radiation. This approach requires the development of contrast agents responsive to copper and zinc, that is, probes whose MRI signal will vary as a function of binding to or reacting with the two transition metals. Importantly, copper and zinc can accumulate *in vivo* in high concentration of up to hundreds of μM.[8-17] They are thus good targets for MRI contrast agents which are typically also used *in vivo* at similar concentrations. Indeed, it is because the concentrations of the labile metal ions in certain pathologies are in the range of the sensitivity of MRI contrast agents that they have been successfully used to image changes in the labile zinc pool levels in the pancreas[13, 14] as well as in prostate cancer.[15, 16] They have also been successfully used to image zinc levels in the brain[17] despite not being able to pass the blood brain barrier.

Current responsive contrast agents for copper and zinc are almost all based on gadolinium complexes.[18] Two strategies have been employed successfully in the design of this class of responsive MR probes: *q*-based agents, whereby the relaxivity of the complex is modulated by the number of inner-sphere water molecules, *q*, and τ_R-based agents, where it is instead modulated by the rotational correlation time of the Gd-H vector, τ_R. According to the Solomon-Bloembergen-Morgan (SBM) theory which governs the relaxivity of gadolinium complexes, their longitudinal relaxivity r_1 is directly proportional to the number of inner-sphere water molecules, *q*. Responsive probes for metal ions have thus been designed by incorporating a chelating moiety that binds directly to the Gd^{3+} ion in the absence of zinc or copper, but releases the lanthanide upon chelation of the transition metal. As the open coordination site is replaced by water, *q* increases and so does r_1. This approach has been used successfully for all copper-responsive T_1-based MR probes,[19-26] as well as for a number of zinc-responsive contrast-agents.[27-35] The second approach, which thus far has only been applied to Zn^{2+}, involves the formation of a Zn^{2+}-templated macromolecule, either *via* the formation of a dimer[36-39] or upon binding to human serum albumin (HSA).[14, 40, 41] In either case, the Gd-H vector in the resulting macromolecule has longer rotational correlation time,

[a] *K. Srivastava, S. Harris, V. C. Pierre- Department Department of Chemistry, University of Minnesota, Minneapolis MN 55455, USA*
E-mail: pierre@umn.edu
[b] *G. Ferrauto, D. L. Longo, S. Aime - Molecular Imaging Center, Department of Molecular Biotechnologies and Health Sciences, University of Torino, 10126 Torino, Italy*
[c] *M. Botta. Dipartimento di Scienze e Innovazione Tecnologica, Università del Piemonte Orientale "Amedeo Avogadro", 15121 Alessandria, Italy*
† Equal contributions
Electronic Supplementary Information (ESI) available: ^{1}H-NMR spectra of Tm-DOTAm-py (14 T, 10 °C) in H_2O and D_2O and in presence of Zn^{2+} showing exchangeable protons, Z- and ST% spectra of Tm-DOTAm-py and Tm-DOTAm-βAla-py upon addition of Cu^{+}, Cu^{2+}, and Zn^{2+}, Z- and ST% spectra of Eu-DOTAm-py, - and ST% spectra of Tm-DOTAm-py at pH 7.4 and 10.3, CEST phantom MR images of Tm-DOTAm-py in the absence and presence of Cu^{+}, Cu^{2+}, and Zn^{2+}, τ_M of Tm-DOTAm-py upon addition of Cu^{2+}, NMR spectra of final ligands and metal complexes. See DOI: 10.1039/x0xx00000x

τ_R, than the monomeric Gd^{3+} complex and thus, as predicted by the SBM theory, substantially higher r_1.

None of the responsive T_1-based agents for Zn^{2+} have shown any selectivity for copper. Importantly, this lack of selectivity does not prohibit *in vivo* applications. Zinc-responsive contrast agents that were not demonstrated to be selective over copper were successfully used to image the pancreas[13, 14] and prostate cancer.[15, 16] Nonetheless, a number of general conclusions can be learned from these studies. The first is that *q*-based contrast agents typically do not result in a substantial increase in r_1, typically less than two-fold, although in some cases three fold increases have been observed. τ_R-based responsive probes that rely on binding to large proteins such as HSA have higher turn-on responses, although, as predicted by the SBM theory, such a turn-on is dependent on the magnetic field strength of the MR instrument.[14, 40, 41] Second, the response of *q*-based contrast agents can be significantly affected by the presence of endogenous anions that can also replace the inner-sphere water molecule(s), particularly phosphate and bicarbonate. This effect can be attenuated by increasing the negative charge of the Gd^{3+} complex, for instance *via* the attachment of pendant carboxylate arms.[20] Practically, given that these contrast agent do not distribute uniformly throughout a tissue, let alone a body, the poor response of these probes can render their *in vivo* application problematic, particularly at high fields.

Not all responsive contrast agents for transition metals are gadolinium-based.[18] Iron oxide nanoparticles can also be rendered responsive to labile transition metals if they are coated with polymers that are terminated by functional groups that either chelate to or react with copper or zinc. In this case, the formation of clusters of monocrystalline iron oxide nanoparticles (MIONs) results in a decrease in the longitudinal relaxivity, r_1, of the nanoparticles and a change in their transverse relaxivity, r_2. This strategy has been successfully applied to the detection of Cu^+.[42, 43] No MION-based responsive contrast agent has been reported for Zn^{2+} so far. In any case, the weak response of particulate responsive contrast agents remain problematic.

Another class of responsive contrast agents is based on chemical exchange saturation transfer (CEST) agents.[18] CEST agents are a class of MRI contrast agents that function by decreasing the intensity of *bulk* water signal upon selectively saturating the resonance frequency of the mobile proton of the agent, either belonging to coordinated water molecule(s), or to NH or OH groups.[44] Given that the effectiveness of a CEST contrast agent is determined in part by the chemical shift difference ($\Delta\omega$) between water and the exchangeable ^1H, paraCEST agents which contain a paramagnetic metal that shifts the exchangeable proton(s) further away from *bulk* water signal show improved sensitivity.[45, 46] This is due in part to the fact that such systems can use protons with faster exchange rate (k_{ex}) since the larger $\Delta\omega$ prevents coalescence with the signal from *bulk* water. Moreover, since their proton resonance is at a frequency shifted far from the endogenous signals of tissues, paraCEST agents have the added advantages of smaller background signal interference. These agents can be rendered responsive either by changing the number of exchangeable protons (in a similar manner as *q*-based Gd^{3+} probes), or by changing the exchange rate of the labile proton ($k_{ex} = 1/\tau_M$). Following this strategy, responsive CEST and paraCEST agents have been reported for a wide variety of targets, such as pH, enzymes, ions, and temperature.[47, 48]

Two CEST responsive MRI contrast agents for Zn^{2+} have been reported by Bulte J.W.M. and Sherry A.D.[49-51] These probes were not evaluated toward copper, so their selectivity toward the isoelectronic Cu^+ is unknown. In Sherry's probe, a 50% reduction in relative CEST magnitude of that probe is observed upon addition of 20 mM Zn^{2+}.[51] This probe yields a similar change in signal intensity but at notably higher concentration of Zn^{2+} than the Gd^{3+}-based contrast agents mentioned above. Bulte's CEST probe is more sensitive and can detect 200 μM Zn^{2+} but with a smaller CEST effect (10%), although no titration or binding affinity are reported.[49] No CEST agents for either Cu^+ or Cu^{2+} have yet been reported.

With this in mind, and based on the copper responsive Gd^{3+} contrast agents developed by the Chang group[19] we designed and tested two responsive paraCEST agents for copper and zinc, Tm-DOTAm-py and Tm-DOTAm-βAla-py (Figure 1). Both of these probes incorporate three amides with exchangeable protons together with the pyridine-thioether chelating group previously used by Chang and coworkers to detect Cu^+ selectively in a Gd^{3+} q-based contrast agent.[19] These amides provide three exchangeable protons distinctly positioned away from any possible inner-sphere water molecules. The initial concept was that upon coordinating copper or zinc via the pyridine moiety, either the number of inner sphere water molecule or the exchange rate of the amide protons would change, and therefore, so would the intensity of the CEST image and the % saturation transfer. Following previous work by Chang,[20] Tm-DOTAm-py was further functionalized with three negatively charged β-alanine moieties whose role was to decrease possible interference by endogenous anions by eliminating the positive charge of the Tm-DOTAm-py complex.

Results and Discussion

The ligand DOTAm-py was synthesized according to Scheme 1 starting from 2,2',2''-(1,4,7,10-tetraazacyclododecane-1,4,7-triyl)tris(*N*-methylacetamide) (**1**), a precursor prepared in five steps according to literature protocol.[52, 53] Alkylation of the trisamide **1** with 2,6-bis(chloromethyl)pyridine produced **2**, which was then reacted with 3,9-dithia-6-monoazaundecane (previously prepared according to literature procedure)[54] in the

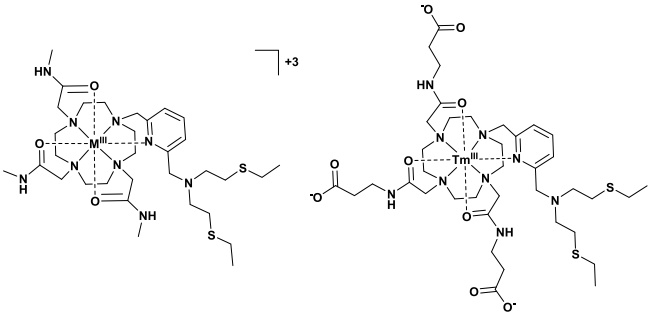

Fig. 1 Chemical structures of the positively charged Ln-DOTAm-py (M = Tm^{3+}, Eu^{3+}, and Gd^{3+}, *left*) and of the neutrally charged Tm-DOTAm-βAla-py (*right*).

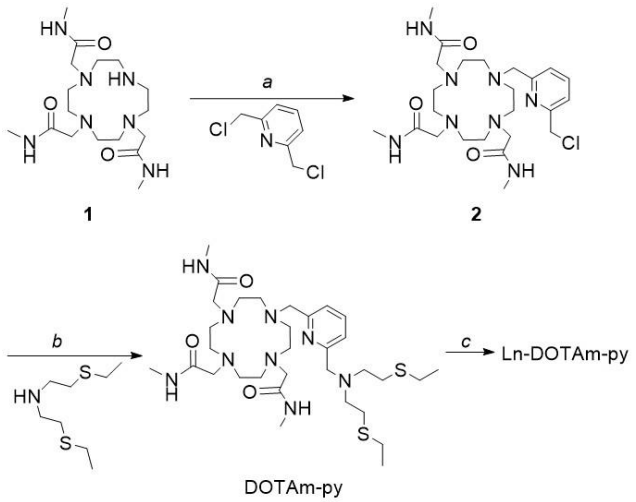

Scheme 1 Synthesis of Tm-, Eu-, and Gd-DOTAm-py. Reagents and conditions: (a) CH_3CN, Cs_2CO_3, 68 °C, 40 h, 29%; (b) CH_3CN, Cs_2CO_3, 68 °C, 40 h, 67%; (c) MCl_3 (M = Tm, Eu, Gd), NaOH (aq), H_2O: CH_3OH (1:1), pH~7, 70 °C, 72-75 h; 86-87%.

presence of Cs_2CO_3 to yield the final ligand DOTAm-py. Finally, the Tm^{3+}, Eu^{3+}, and Gd^{3+} complexes of DOTAm-py were prepared by treating the ligand with 1 equivalent of the corresponding metal chloride salt in a 1:1 water: methanol mixture regularly adjusted to neutral pH by addition of aqueous NaOH. Note that due to the inert nature of macrocyclic lanthanide complexes, the metalation reaction must be refluxed for at least three days to ensure full complexation of the lanthanide ion. Residual free lanthanide ion was removed by filtration following precipitation at alkaline pH. The absence of residual free lanthanide ion was confirmed by complexometry with xylenol orange metal indicator. The concentration of the lanthanide complexes in aqueous solutions was determined by Evan's method.[55]

The second paraCEST probe Tm-DOTAm-βAla-py was synthesized according to Scheme 2 from the same monoprotected cyclen precursor **3** which was instead alkylated with *tert*-butyl 3-(2-chloroacetamido)propanoate in the presence of Cs_2CO_3. Hydrogenation of the resulting intermediate **4** in the presence of Pd/C yielded the trisubstituted cyclen **5**, similar to synthesis schemes in literature.[56, 57] This intermediate was further functionalized with the metal-responsive unit *N*-((6-(chloromethyl)pyridin-2-yl)methyl)-2-(ethylthio)-*N*-(2-ethylthio)ethan-1-amine to yield the ester-protected ligand DOTAm-βAla-py (**6**). The pendant arm and the pyridine chelating arm were both previously synthesized as reported in the literature.[19, 58] Deprotection of the carboxylic acids with trifluoroacetic acid at 0 °C yielded the final ligand DOTAm-βAla-py which was metalated with $TmCl_3$ at neutral pH to give the final probe, Tm-DOTAm-βAla-py.

An extensive characterization of the Ln-DOTAm-py and Tm-DOTAm-βAla-py agents was carried out with the aim of assessing and understanding the response of the lanthanide probes to copper and zinc. These include both the evaluation of the CEST spectra of the Tm^{3+} and Eu^{3+} complexes as well as the relaxometric properties of the Gd^{3+} analogue.

In the absence of copper or zinc and at physiological pH, Tm-DOTAm-py displays one rather broad CEST signal centered at -98 ppm (Figure 2a). In order to assess the origin of the CEST signal, ^{1}H NMR spectra of Tm-DOTAm-py in H_2O and in D_2O were recorded at 14 T (600 MHz) and 10 °C (Figures 3 and S1). At this temperature, three exchangeable proton pools are visible between -98 and -104 ppm (Figure 3). These signals correspond to the amide protons. They are well separated at low temperature but broader at higher temperatures which indicates an incipient intramolecular dynamic (Figure S1c). As predicted, no inner-sphere water molecules were observed by CEST (Figure 2a and Figure S2). This observation is in agreement with the structural analogous Gd^{3+} complex of Chang in which the three amides are replaced by three carboxylates.[19-21] In all cases, coordination of the pyridine to the lanthanide does not allow for an inner-sphere water molecule.

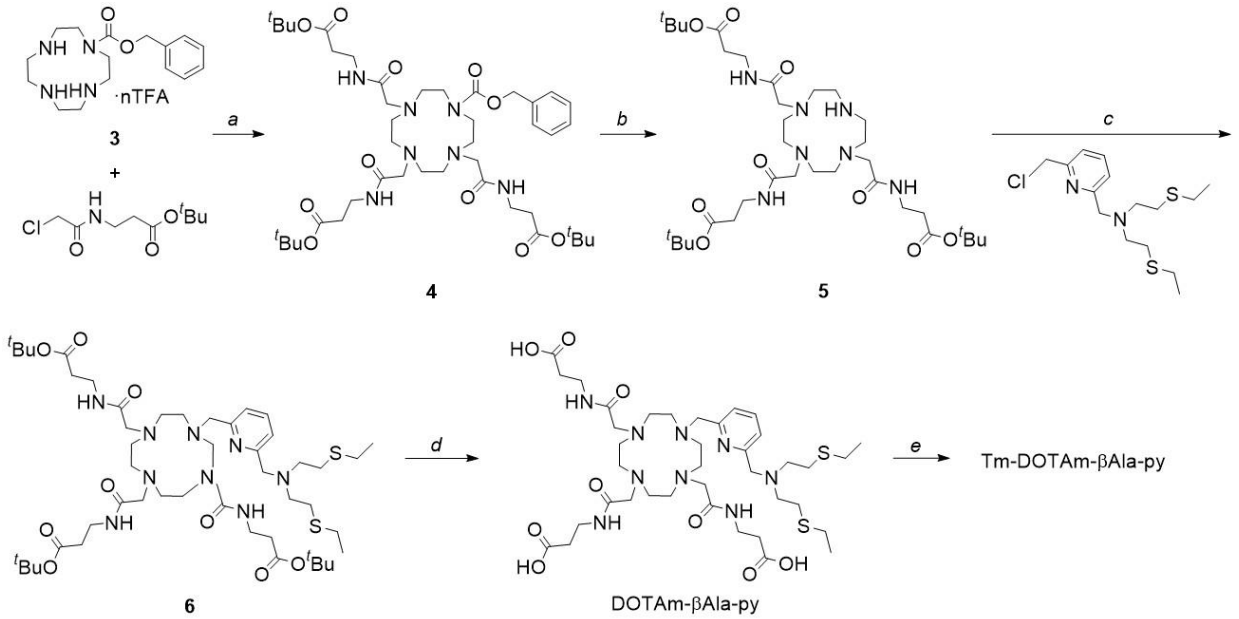

Scheme 2 Synthesis of Tm-DOTAm-βAla-py. Reagents and conditions: (a) CH_3CN, Cs_2CO_3, 55 °C, 36 h, 81%; (b) H_2, Pd/C, 50 psi, CH_3OH, rt, 24 h; (c) CH_3CN, Cs_2CO_3, 70 °C, 40 h, 43%; (d) TFA, DCM, 0 °C-rt, 24 h, 70%; (e) $TmCl_3$, NaOH (aq), H_2O: CH_3OH (2:1), pH~7, 70 °C, 72 h; 94%.

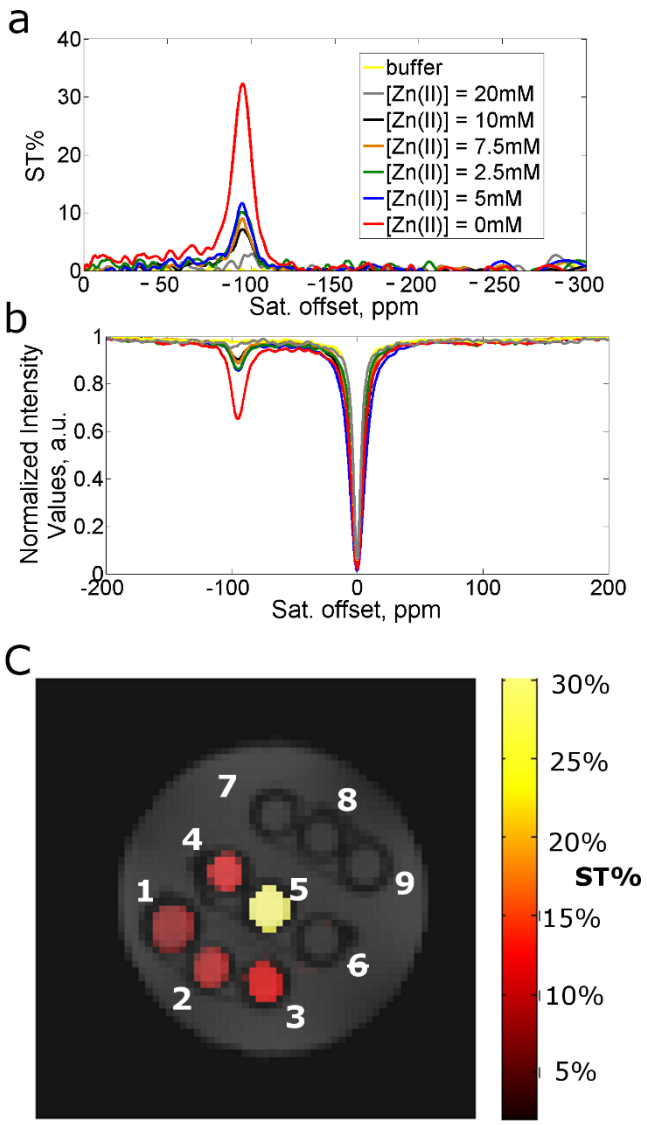

Fig. 2 a) Saturation transfer % (ST%) spectra and b) Z-spectra of Tm-DOTAm-py upon addition of different concentration of Zn^{2+}. Experimental conditions: [Tm-DOTAm-py] = 10 mM, [HEPES] = 3.8 mM, pH = 7.2, B1 = 24 μT, T = 21 °C. c) CEST-MR image of phamtom containing glass capillaries filled with: 1) Tm-DOTAm-py 10 mM + Zn^{2+} 10 mM, 2) Tm-DOTAm-py 10 mM + Zn^{2+} 7.5 mM, 3) Tm-DOTAm-py 10 mM + Zn^{2+} 5 mM, 4) Tm-DOTAm-py 10 mM + Zn^{2+} 2.5 mM, 5) Tm-DOTAm-py 10 mM, 6) Zn^{2+} 10 mM, 7) Zn^{2+} 7.5 mM, 8) Zn^{2+} 5 mM, 9) Zn^{2+} 2.5 mM.

Interestingly, whereas Tm-DOTAm-py shows a strong CEST effect, its analogue Eu-DOTAm-py complex does not display a noticeable one (Figure S3). This is likely due to the lower shift provided by Eu^{3+} in respect to Tm^{3+} and highlights the large effect that a seemingly small change in the composition of a CEST probe can have on its response.

Addition of Cu^{+}, Cu^{2+}, or Zn^{2+} leads to the complete disappearance of the CEST signal. As shown in Figure 2a and b, the Z-spectra and percent saturation transfer (ST%) spectra of Tm-DOTAm-py decrease substantially upon gradual addition of Zn^{2+}. Similar spectra were obtained upon addition of Cu^{+} and Cu^{2+} (Figure S4-S5). A CEST-MR image of a phantom containing glass capillaries filled with 10 mM Tm-DOTAm-py (*aq*) and 0-10 mM Zn^{2+} (*aq*) is shown in Figure 2c. As controls, capillary tubes 6 to 9 contain Zn^{2+} (*aq*) but no Tm^{3+} complex. No CEST signal is detectable in those tubes, confirming that the CEST signal arises from the Tm^{3+} complex. As can be observed in the MR image, the CEST contrast is more pronounced in the absence of Zn^{2+} and progressively disappears upon addition of the transition metal. This image mirrors the ST% and Z-spectra data obtained for Tm-DOTAm-py upon addition of Zn^{2+} (Figure 2a,b). Similar phantom images were obtained for Tm-DOTAm-py upon addition of varying concentrations of either Cu^{+} or Cu^{2+} (Figure S6-S7). These phantom images confirm that Tm-DOTAm-py can be used to image changes in the concentration of labile copper or zinc.

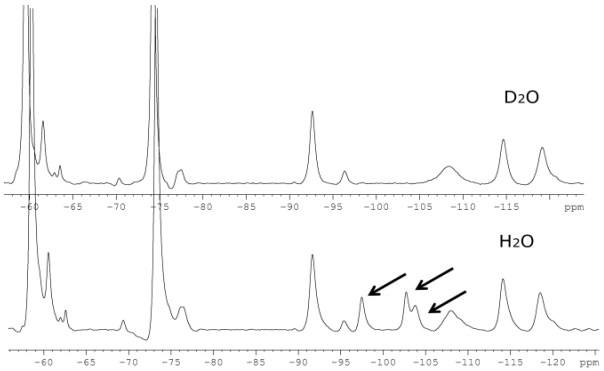

Fig. 3 ^{1}H-NMR spectra of Tm-DOTAm-py (14 T, 10 °C) in H_2O and D_2O showing exchangeable protons.

The ST% of Tm-DOTAm-py disappears upon addition of either Cu^{+}, Cu^{2+}, or Zn^{2+} (Figures 2, S4 and S5), suggesting that the coordination of the transition metal affects the exchange rate of the mobile proton. τ_M of mobile protons of Tm-DOTAm-py was measured to be *ca*. 100 μs via the Omega plot method (Figure S8). Addition of copper or zinc does increases the exchange rate of the mobile protons and decreases τ_M to *ca*. 30-50 μs for the Tm-DOTAm-py:Cu^{2+} adduct and Tm-DOTAm-py:Zn^{2+} adduct (Figure S8). Addition of Cu^{+} leads to a smaller effect on τ_M than Cu^{2+} and Zn^{2+}. The increase in amide protons exchange rates is further confirmed by the ^{1}H NMR spectra of Tm-DOTAm-py in the presence of an equivalent of Zn^{2+} (Figure S1d). The amide proton resonances progressively broaden upon addition of Zn^{2+} to Tm-DOTAm-py (*aq*). Thus, the disappearance of the CEST signal upon addition of either zinc or copper likely arises from the increase of the exchange rate of the amide protons.

Interestingly, no new CEST signal corresponding to an inner-sphere water molecule was observed upon addition of either copper or zinc. This observation suggests that the coordination environment of the Tm^{3+} center does not change upon addition of copper or zinc, that is, the pyridine remains coordinated to the Tm^{3+} and does not bind copper or zinc.

Further evidence for the mechanism of action of our probe and for the lack of change in the coordination environment of the lanthanide ion upon formation of a zinc or copper adduct was obtained from proton relaxometric experiments. First, the relaxivity of Gd-DOTAm-py was evaluated in the absence and presence of diamagnetic Zn^{2+}. The observed r_1 value of Gd-DOTAm-py at neutral pH and room temperature (2.26 mM^{-1} s^{-1} at 0.47 T) (Figure 4) is low and strongly indicative of the absence of any water molecule in the inner coordination sphere of the

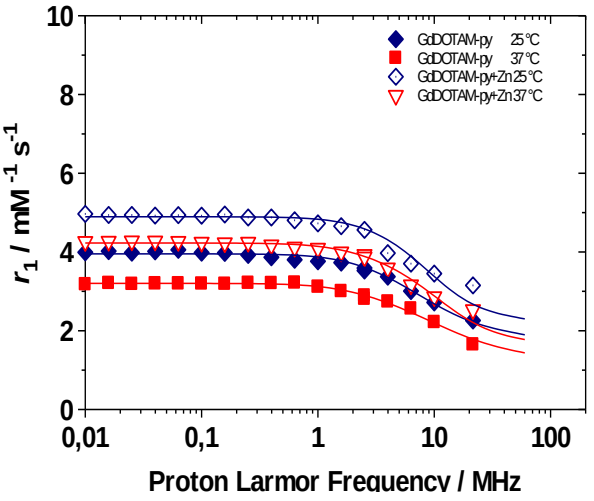

Fig. 4 Longitudinal relaxivity ^{1}H NMRD profile of Gd-DOTAm-py in the absence (filled symbols) and presence (open symbols) of 2 equivalents of Zn^{2+} at 25 °C (blue symbols) and 37 °C (red symbols).

metal ion (q = 0). In fact, this relaxivity value corresponds exactly to that measured for $[Gd(TTHA)]^{3-}$ (H_6TTHA = triethylenetetraminehexaacetic acid), a complex which also does not contain any inner-sphere water molecule,[59] and to the outer sphere relaxivity calculated for Gd-DOTA.[60] In aqueous solution and at neutral pH, the Gd^{3+} ion in the cationic Gd-DOTAm-py is therefore in an octacoordinated ground state and the observed relaxivity is only the result of the outer-sphere relaxation mechanism.

In the presence of Zn^{2+}, although the longitudinal relaxivity increases by *ca*. 40% (3.15 $mM^{-1} s^{-1}$ at 0.47 T), its value is still low enough to rule out any contribution from a Gd-bound H_2O molecule. However, the increase in r_1 indicates that the lack of a coordinated water molecule is partly compensated by the presence of a number of water molecules hydrogen-bonded to the polar groups of the ligand, with a residence lifetime sufficiently long and at a distance sufficiently short from the Gd^{3+} to contribute to the observed relaxivity (second sphere mechanism).[61]

The ^{1}H $1/T_1$ NMRD profiles were recorded at both 25 °C and 37 °C in absence and presence of Zn^{2+} (Figure 4). For Gd-DOTAm-py, the curves were fitted according to the Freed equation for the outer-sphere contribution to relaxivity.[62] The best-fit parameters, which are reported in Table 1, are fully in line with those of other macrocyclic q = 0 Gd^{3+} complexes.[63] The NMRD profiles of Gd-DOTAm-py in the presence of Zn^{2+} have been analysed considering a contribution from both *outer*- and *second sphere* (SS) hydration. The number of SS water molecules (q') has been arbitrarily fixed to 2 because this assumption allows to obtain a very plausible value of the distance r' (3.82 Å) from the metal center. The other parameters were allowed to vary within a reasonable range of values. The magnetic field-dependence of r_1 is well reproduced in terms of a sizeable contribution of two H-bonded water molecules at a distance of 3.82 Å from the paramagnetic ion, with a residence lifetime of *ca*. 1 ns. The parameters of the electronic relaxation have values quite similar to those reported for other DO_3A-

Table 1 Refinement parameters for the $1/T_1$ NMRD profile of Gd-DOTAm-py in the absence and presence of Zn^{2+}.

	Gd-DOTAm-py		Gd-DOTAm-py +Zn^{2+}		GdDOTA[a]
T (°C)	25	37	25	37	25
r_1 ($mM^{-1} s^{-1}$)	2.26	1.65	3.15	2.53	2.33[b]
Δ^2 (s^{-2}; $\times10^{19}$)	3.0	3.0	3.7	3.7	1.6
τ_V (ps)	18	13	17	11	11
q'	/	/	2	2	/
r' (Å)	/	/	3.82	3.82	/
τ_R' (ps)	/	/	29	23	/
τ_M' (ns)	/	/	1	0.8	/
a (Å)	4.0	4.0	4.20	4.20	3.7[c]
D ($cm^2 s^{-1}$;$\times10^5$)[c]	2.24	3.10	2.24	3.10	2.2

[a] ref.[63]; [b] outer sphere contribution; [c] fixed during the fit.

derivatives and do not vary significantly upon Zn^{2+} binding.[64]

The absence of any inner-sphere water molecule was further confirmed by ^{17}O NMR transverse relaxation rates (R_2) and paramagnetic shifts ($\Delta\omega$) of aqueous solutions of Gd-DOTAm-py in the presence and absence of Zn^{2+} as a function of temperature. As can be seen in Figure 5, the data obtained unambiguously indicate the lack of water molecules in the inner coordination sphere of the complex, both before and after the addition of Zn^{2+}. In fact, the experimental data of the

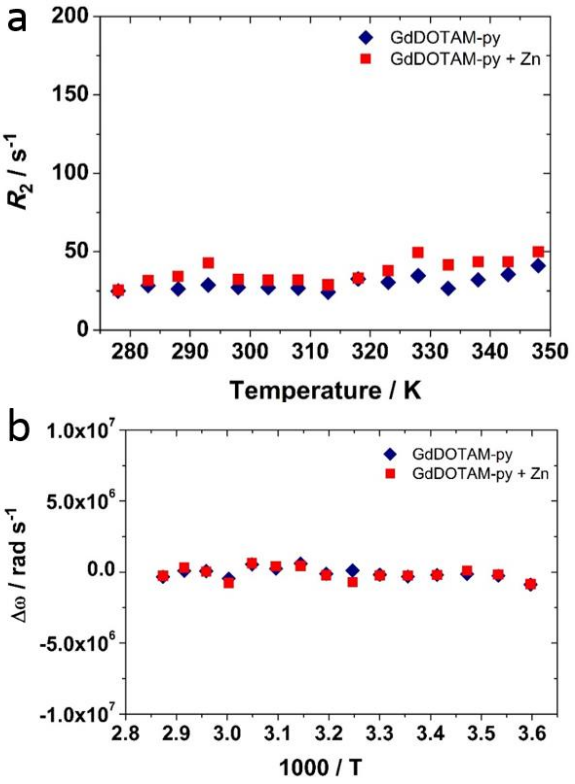

Fig. 5 a) ^{17}O NMR transverse relaxation rates (R_2) and b) paramagnetic shifts ($\Delta\omega$) of Gd-DOTAm-py as a function of temperature in the absence (blue) and presence (red) of 2 equivalents of Zn^{2+}. Experimental conditions: [Gd-DOTAm-py] = 7.4 mM, B = 11.4 T.

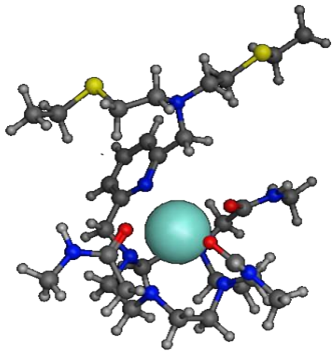

Fig. 6 The lowest energy conformation of Gd-DOTAm-py obtained by molecular modelling shows reduced accessible surface area to coordinate a water molecule.

paramagnetic Gd^{3+} complex solution are barely distinguishable from the diamagnetic reference solution.

Further evidence of the absence of coordinated water molecules was obtained by molecular modelling simulations. A calculated *q*-value of 0.21 was obtained, based on the accessible surface area of the minimum energy conformation of the Gd-DOTAm-py complex. The calculated lowest energy conformation shows a high steric hindrance around the Gd^{3+} ion that hampers the entrance of a water molecule to the inner coordination sphere (Figure 6). This result is in agreement with the NMRD data, as well as with the ^{17}O NMR transverse relaxation rates (R_2) and paramagnetic shifts (Δω) experiments discussed above.

Altogether, CEST, NMRD and ^{17}O NMR experiments all specify that Tm-DOTAm-py does not have an inner-sphere water molecule even in the presence of copper or zinc. This indicates that the pyridine group coordinates Tm^{3+} even in the presence of the transition metals. Moreover, in the titration of Tm-DOTAm-py with Zn^{2+} and Cu^{2+}, the ST% plateaus at approximately 0.5 equivalent of transition metal (Figure 7). This observation strongly suggests the formation of a 2 Tm- DOTAm-py: 1 Zn^{2+} or a 2 Tm-DOTAm-py: 1 Cu^{2+} assembly similar to that observed by Chen for his Zn^{2+}-responsive Gd^{3+} contrast agent[36]

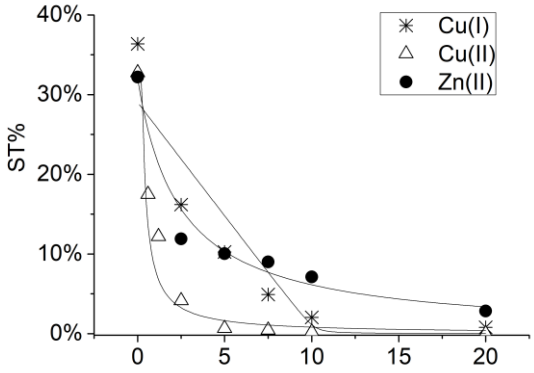

Fig. 7 Percent saturation transfer, ST%, of Tm-DOTAm-py upon addition of $[Cu(CH_3CN)_4]PF_6$, $CuCl_2$, or $ZnCl_2$. Solid represent the fit to the equilibriums described in Table 2. Experimental conditions: [Tm-DOTAm-py] = 10 mM, [HEPES] = 3.8 mM, pH = 7.2, B1 = 24 μT, T = 21 °C.

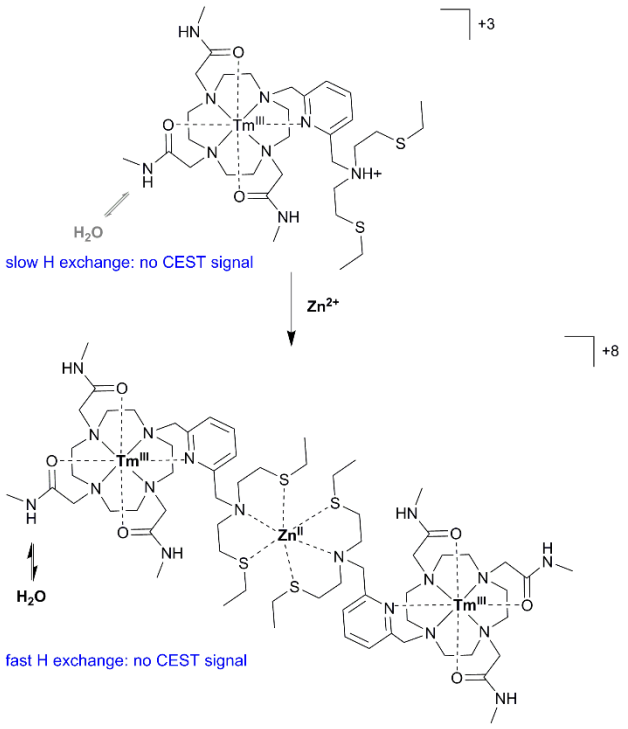

Fig. 8 Proposed mechanism of CEST response of Tm-DOTAm-py to Zn^{2+}.

and a 1:1 Tm^{3+}: Cu^{+} complex. Altogether, these results suggest the formation of a copper or zinc-templated dimer as shown in Figure 8.

Although the mechanism of response of Tm-DOTAm-py to Zn^{2+} is the same as that of Sherry's Eu^{3+}-based Zn^{2+} CEST probe, Tm-DOTAm-py has a substantially greater turn-off than Sherry's europium probe.[51] For Tm-DOTAm-py, the ST% decreases from 33% to nearly 0% upon addition of 2 equivalents of Zn^{2+} (Table2), whereas in the Sherry's Eu^{3+}-based probe, a smaller (50%) reduction in CEST signal from 27% to 14% was observed upon addition of 20 mM Zn^{2+}. This higher response to "free"

Table 2 Apparent association constants, K_a, and % saturation transfer of free and metal-bound Tm-DOTAm-py and Tm-DOTAm-βAla-py.[a]

		Tm-DOTAm-py	Tm-DOTAm-βAla-py
$ST\%_{free}$		33.8	9.3
$ST\%_{bound}$		0	0
Cu(I)			
K_{CuL}	$Cu^{+} + L \leftrightarrows [CuL]^{+}$	7.7×10^{4}	1.6×10^{4}
Cu(II)			
K_{CuL}	$Cu^{2+} + L \leftrightarrows [CuL]^{2+}$	2.8×10^{7}	3.9×10^{7}
K_{CuL2}	$[CuL]^{2+} + L \leftrightarrows [CuL_2]^{2+}$	2.8×10^{3}	9.9×10^{3}
Zn(II)			
K_{ZnL}	$Zn^{2+} + L \leftrightarrows [ZnL]^{2+}$	3.0×10^{6}	1.2×10^{6}
K_{ZnL2}	$[ZnL]^{2+} + L \leftrightarrows [ZnL_2]^{2+}$	2.4×10^{5}	1.4×10^{5}

[a] Experimental conditions: [Tm-DOTAm-py] = 10 mM or [Tm-DOTAm-βAla-py] = 5 mM, [HEPES] = 3.8 mM, pH 7.2, B_1 = 24 μT for Tm-DOTAm-py and 48 μT for Tm-DOTAm-βAla-py, T = 21°C.

metal ion is expected to make Tm-DOTAm-py a better candidate for imaging zinc levels in pancreatic cancer.[65]

As can be seen from the titration data and associated binding affinity shown in Figure 7 and Table 2, Tm-DOTAm-py binds Cu^{2+} with higher affinity than Cu^{+} and Zn^{2+} but with essentially no selectivity. These results align with those of other *q*-based gadolinium responsive contrast agent for Zn^{2+} which also showed no or nearly no selectivity over copper.[22-30] (Note that the selectivity of the other reported CEST probe for Zn^{2+} was not assessed). This observation is, however, in contradiction with the chemically analogous Gd^{3+} complex developed by the Chang group and which was reported to be highly selective for Cu^{+} over both Cu^{2+} and Zn^{2+}.[20] It should be noted, however, that the structural change to the probe upon formation of the ternary complex with the transition metal is very different in the case of the Gd^{3+} complex of Chang than that of our Tm^{3+} CEST probe. In the presence of copper, the pyridine moiety of the Gd^{3+} triscarboxylate complex of Chang does not coordinate the lanthanide ion but instead binds copper. This is not the case for the Tm^{3+} trisamide complex (Tm-DOTAm-py) for which the pyridine moiety does not uncoordinate the lanthanide in the presence of copper (Figure 8).

The neutral analogue of Tm-DOTAm-py, Tm-DOTAm-βAla-py, which contains three pendant negatively charged carboxylate arms, shows a similar response to Cu^{+}, Cu^{2+}, and Zn^{2+} (Figure 9, see Figures S9-S11 for Z- and ST% spectra). The apparent association constant of the neutral probe for the transition metals shown in Table 2, are comparable, albeit a little weaker, than that of the positively charged Tm-DOTAm-py. This suggests that any benefit from removing the positive charge of the complex with pendant carboxylate groups (which usually increases K_a) is likely countered by increased steric hindrance. Both probes bind Cu^{2+} with higher affinity than Zn^{2+} in accordance with the Irving-Williams series. Unfortunately, the addition of the three carboxylate arms substantially decreases the magnitude of the CEST effect (compare ST = 33% with a B_1 = 24 μT for 10 mM of Tm-DOTAm-py versus ST = 9% with a B_1 = 48 μT for 5 mM Tm-DOTAm-βAla-py). Similar effect has been observed previously by Hudson et al. by replacing the alkyl amide substituent with terminal carboxylic groups to reduce the overall positive charge on the Tm^{3+} complex to increase their biocompatibility.[66] Such a large decrease in the ST% for the neutral versus the positively charged complex indicates that the neutrally charged Tm-DOTAm-βAla-py is not a viable option for *in vivo* imaging of the labile pools of transition metals.

The affinity constants K_a of Tm-DOTAm-py and Tm-DOTAm-βAla-py for Cu^{2+} are higher than that of other Gd probes which have an iminodiacetate arm ($K_a = 5.9\times10^3$ M^{-1}),[67] including Nap-DO3A-Gd ($K_a = 8.5\times10^4$ M^{-1})[26] and $[Gd(Try\text{-}TTDA)(H_2O)]^{2-}$ ($K_a = 4.0\times10^2$ M^{-1}).[25] However, it is much lower than that of Gd probes with acetate-thioether arms ($K_a = 1.0\times 10^{15}$ M^{-1}).[19] The binding affinities of both probes for Cu^{+} is noticeably lower that of chemically analogous probes from Chang ($K_a \sim 10^{11}$ to 10^{15} M^{-1}).[19, 20] This observation is in agreement with our proposed mode of action for Tm-DOTAm-py and Tm-DOTAm-βAla-py in which, unlike Chang's probe, the pyridine moiety does not release the Tm^{3+} ion to bind Cu^{+}, resulting in a weaker Cu^{+} complex. Tm-DOTAm-py also binds Zn^{2+} with an affinity higher than that of the Gd responsive contrast agent, Zn-Gd-daa3 ($K_a = 4.2\times10^3$ M-1).[27] Its cumulative formation constant $\beta_{ZnL2} = K_{ZnL} \times K_{ZnL2}$ (7.2×10^{11}) is even higher than that of the other paraCEST agent ($K_a = 3.9\times10^7$ M^{-1}).[51]

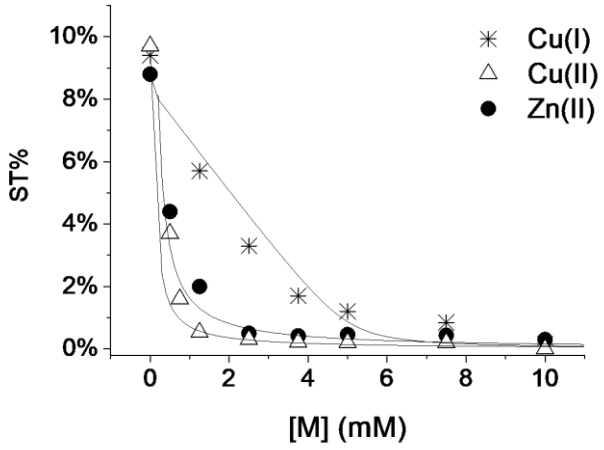

Fig. 9 Percent saturation transfer, ST%, of Tm-DOTAm-βAla-py upon addition of $[Cu(CH_3CN)_4]PF_6$, $CuCl_2$, or $ZnCl_2$. Solid represent the fit to the equilibriums described in Table 2. Experimental conditions: [Tm-DOTAm-βAla-py] = 5 mM, [HEPES] = 3.8 mM, pH = 7.2, B_1 = 48 μT, T = 21 °C.

Conclusions

Two thulium complexes, Tm-DOTAm-py and Tm-DOTAm-βAla-py, have been synthesized and evaluated as responsive paraCEST MRI probes for the detection of the transition metals Cu^{+}, Cu^{2+} and Zn^{2+}. Tm-DOTAm-py is positively charged, whereas the three pendant carboxylate arms of Tm-DOTAm-βAla-py neutralizes the charge of the latter. In both cases, the CEST signal arises from the amide groups. Notably, Tm-DOTAm-py is a more sensitive CEST agent than Tm-DOTAm-βAla-py with a higher ST%. The CEST effect of both probes is completely eliminated upon binding Cu^{+}, Cu^{2+}, or Zn^{2+}, consistent with a change in the exchange rates of amides. Notably, unlike for its Gd^{3+} *q*-based contrast agent analogues, the pyridine moiety of either probe does not appear to uncoordinate the lanthanide ion upon binding zinc or copper. As such, no inner-sphere water molecules are observed, either by CEST of the Tm^{3+} complex, $1/T_1$ NMRD and ^{17}O NMR of the Gd^{3+} complex or molecular modelling simulations on Gd^{3+} complex. Both probe form a 1:1 complex with Cu^{+} and a 2:1 complex with Cu^{2+} and Zn^{2+} with binding affinity comparable to that of other responsive MRI contrast agents for copper and zinc. The greater response of Tm-DOTAm-py upon binding to the transition metal renders it a promising candidate for the development of a contrast agent for imaging copper and zinc *in vivo*. The binding to transition metal increases the exchange rate of amides' protons to such a degree that the CEST effect disappears. As a result, these probes yield a truly on/off response that is rare for the detection of metal ions by MRI.

Experimental Section

General considerations

Starting materials were obtained from commercial suppliers and used without further purification. 2,2',2"-(1,4,7,10-tetraazacyclododecane-1,4,7-triyl)tris(*N*-methylacetamide) (**1**), benzyl 1,4,7,10-tetraazacyclododecane-1-carboxylate (**3**),[52, 53] 3,9-dithia-6-monoazaundecane,[54] *tert*-butyl 3-(2-chloroacetamido)propanoate,[58] and *N*-((6-(chloromethyl)pyridin-2-yl)methyl)-2-(ethylthio)-*N*-(2-(ethylthio)ethyl)ethan-1-amine[19] were synthesized as previously described in the literature with successful synthesis established by ^{1}H NMR and LR MS. Water was distilled and further purified by a Millipore cartridge system (resistivity 1.8×10^7 Ω.cm). All organic extracts were dried over anhydrous $MgSO_4$ and solvents were removed under reduced pressure with a rotary evaporator. ^{1}H spectra were obtained at room temperature on Varian Inova 500 and 300 at 500 and 300 MHz respectively. ^{13}C NMR spectra were recorded on Varian Inova 500 at 126 MHz at the LeClaire-Dow Characterization Facility of the Department of Chemistry at the University of Minnesota. Data for ^{1}H NMR is reported as follows: chemical shift (δ, ppm), multiplicity (br = broad, s = singlet, d = doublet, t = triplet, m = multiplet), coupling constants (Hz). Data for ^{13}C NMR are reported as chemical shifts (δ, ppm). The residual solvent peak was used as an internal reference for ^{1}H and ^{13}C NMR. A delay time of 30 ms and acquisition time of 64 ms were used for the collection of ^{1}H NMR spectra of the paramagnetic M-DOTAm-py (M = Tm^{3+}, Gd^{3+} and Eu^{3+}) and Tm-DOTAm-βAla-py complexes. Mass spectra (HRMS, high resolution mass spectrometry; ESI-MS, electrospray ionization mass spectrometry) were recorded on a Bruker BioTOF II at the Waters Center for Innovation in Mass Spectrometry of the Department of Chemistry at the University of Minnesota.

CEST MRI

CEST MR Images were recorded at 7.1T on a Bruker Avance 300 spectrometer equipped with a microimaging probe at 21 °C. A typical RARE (Rapid Acquisition with Refocused Echoes) spin–echo sequence (RF = 16) with an echo time of 3.2 ms and a TR value of 5 s was used. An isotropic 64×64 acquisition matrix with a FOV of 10 mm and a slice thickness of 1 mm was used (matrix resolution of 0.156mm/pixel). The whole sequence was preceded by a saturation scheme consisting of a continuous rectangular wave pulse 2 s long with a presaturation radiofrequency B_1 intensity of 24 or 48 μT. The first B_1 value was preferred because it is compatible with eventual *in vivo* applications, without the SAR issue. The higher B_1 value was chosen for Tm-DOTAm-βAla-py CEST effect and making possible its detection. It is to be considered that this presaturation pulse is too high for *in vivo* application. A frequency offset range of ± 300 ppm was investigated. Z-spectra were processed by using custom-made software,[68, 69] compiled in the Matlab platform (Mathworks Inc., Natick, MA). They were interpolated by smoothing splines to identify the zero-offset on a pixel-by-pixel basis of the bulk water and, then, to assess the correct ST % value over the entire range of investigated frequency offsets. The magnitude of Saturation transfer (ST) effect was calculated as follows:

$$ST\% = \left(1 - \left(\frac{M_S}{M_0}\right)\right) \times 100$$

where MS is the intensity of the bulk water NMR signal after the irradiation on resonance (Δω) of the mobile proton pool and M_0 is the intensity of the bulk water NMR signal after the irradiation at -Δω.

CEST images were acquired on phantoms consisting of glass capillaries filled with aqueous solution of the paramagnetic complexes (5 or 10 mM, pH = 7.2) with variable amounts of Zn^{2+}, Cu^{+} or Cu^{2+} metals.

Proton exchange rate

Exchange rate constants ($k_{ex} = 1/\tau_M$) of the exchangeable protons was measured by using the Omega plot method as reported by Sherry A. D. et al.[70] In the Omega plots, (Mz/(Mo-Mz) was plotted versus $1/\omega_1^2$ (where ω_1 is expressed in radians/second). The *bulk* water signal intensity measurements were carried out at the steady state, after the application of presaturation pulses at different B_1 values (from 12 to 42 μT). The τ_M value is obtained by as follows: $\tau_M = \sqrt{-x_0}$, where x_0 is the X-axis intercept. Each linear plot, obtained by using at least 5 points, showed a $R^2 \geq 0.99$. τ_M was measured at physiological pH upon addition of different amount of Cu^{+}, Cu^{2+} or Zn^{2+}.

Computational modeling

All modeling and docking procedures were carried out using the MOE molecular modeling package (MOE, version 2004.03, Chemical Computing Group Inc., Montreal, Canada). The structures of the chelate of Gd-DOTAm-py was built from the crystal structure of the DOTAM-type chelates obtained from the Cambridge Structural Database (entry code EHOVAY; www.ccdc.cam.ac.uk/) and modeled using the Moe-Builder module keeping the Gd^{3+} coordination cage fixed. Minimization was achieved by a multistep procedure, until convergence was less than 0.0001 kcal mol^{-1} $Å^{-1}$. For all the calculations a modification of the Amber99 force field[71] was used with in-house parametrization to treat gadolinium complexes within the framework of the ionic method.[72-74] Estimation of the number of bound waters in Gd(III) complex was obtained by calculating the exposed Van der Waals surface area in energy-minimized structures.[75]

^{1}H NMRD and ^{17}O NMR Measurements

The exact concentration of the aqueous solutions for ^{1}H NMRD and ^{17}O NMR measurements was determined by the BMS shift method at 11.7T[55] The field-dependent water proton $1/T_1$ longitudinal relaxation rates were measured at 25 °C and 37 °C by using a fast field-cycling Stelar Relaxometer over a continuum of magnetic field strengths from 0.00024 to 0.47 T (corresponding to 0.01-20 MHz proton Larmor frequencies). The relaxometer operates under computer control with an absolute uncertainty in $1/T_1$ < 1%. The temperature was controlled with a Stelar VTC-91 airflow heater equipped with a

copper–constantan thermocouple (uncertainty ±0.1°C). Additional data point at 21.5 MHz was obtained by using the Stelar Spinmaster spectrometer (Stelar, Mede, Pavia, Italy) by mean of the standard inversion-recovery sequence. All experimental $1/T_1$ values were corrected for diamagnetic contributions using a solution of water at pH = 7 and normalized for the Gd-concentration. The concentration of Gd^{3+} in the analyzed solution was assessed by using Evans' method as previously reported.[55]

^{17}O NMR measurements were carried out on a Bruker Avance spectrometer (14.1 T) equipped with a 5 mm probe and standard temperature control unit. Aqueous solution of the complexes (17 mM) contains 2.0% of the ^{17}O isotope (Cambridge Isotope) were used. The observed transverse relaxation rates were calculated from the signal width at half-height.

DOTAm-py-Cl (2).

A solution of 2,2',2''-(1,4,7,10-tetraazacyclododecane-1,4,7-triyl)tris(*N*-methylacetamide) (**1**, 103 mg, 0.267 mmol) and Cs_2CO_3 (94 mg, 0.29 mmol) in acetonitrile (30 mL) was stirred for 10 min at room temperature. Solid 2,6-bis(chloromethyl)pyridine (52 mg, 0.29 mmol) was added to the reaction mixture which was further stirred at 68 °C for 40 h. The mixture was filtered, and the solvent was removed under reduced pressure. The crude solid was purified by chromatography over alumina (neutral), using a gradient of 100% CH_2Cl_2 to 6% CH_3OH in CH_2Cl_2, to give the compound **2** as off-white solid (40 mg, 29%). δH(500 MHz; $CDCl_3$) 8.30 (2H, d, *J* 4.4 Hz), 7.85 (1H, d, *J* 4.4 Hz), 7.63 (1H, t, *J* 7.7 Hz), 7.17 (1H, d, *J* 7.7 Hz), 7.07 (1H, d, *J* 7.4 Hz), 5.20 (1H, t, *J* 6.2 Hz), 4.73 (2H, m), 3.45 (2H, s), 3.21-2.94 (6H, m), 2.81-2.73 (9H, m), 2.72-2.19 (16H, m). δC(126 MHz; $CDCl_3$) 172.1, 171.7, 162.3, 156.9, 137.9, 122.8, 121.1, 65.1, 59.7, 57.4, 56.8, 50.6, 50.3, 26.2, 26.1, 26.0. HR-MS found: $[M+Na]^+$, 547.2864. $C_{24}H_{41}ClN_8NaO_3^+$ calc 547.2882.

DOTAm-py.

A solution of 2,2',2''-(10-((6-((chloromethyl)pyridin-2-yl)methyl)-1,4,7,10-tetraazacyclododecane-1,4,7-triyl)tris(*N*-methylacetamide) (**2**, 40 mg, 0.076 mmol), Cs_2CO_3 (25 mg, 0.076 mmol) and 3,9-dithia-6-monoazaundecane (15 mg, 0.076 mmol) in acetonitrile (20 mL) was stirred at 68 °C for 40 h. The mixture was filtered, and the solvent was removed under reduced pressure. The crude solid was purified by chromatography over alumina (neutral), using a gradient of 100% CH_2Cl_2 to 5% CH_3OH in CH_2Cl_2, to give the compound DOTAm-py as yellowish solid (35 mg, 67%). δH(300 MHz; $CDCl_3$) 8.37 (1H, m), 7.85 (1H,br s), 7.61 (1H, t, *J* 7.6 Hz), 7.54-7.40 (1H, m), 7.15 (1H, m), 3.95 (1H, m), 3.74 (2H, s), 3.44 (2H, s), 3.21-2.94 (6H, m), 2.92-2.29 (37H, m), 1.20 (6H, m). δC(126 MHz; $CDCl_3$) 172.0, 171.6, 171.2, 162.1, 156.4, 137.7, 122.5, 121.6, 60.1, 59.9, 59.1, 58.8, 57.9, 57.7, 57.2, 54.2, 54.1, 53.5, 52.9, 52.2, 51.1, 50.6, 50.4, 29.5, 26.2, 26.0, 14.9. HR-MS found: $[M+H]^+$, 682.4256. $C_{32}H_{60}N_9O_3S_2^+$ calc 682.4255.

General procedure for the synthesis of lanthanide complexes of DOTAm-py. Representative procedure for Tm-DOTAm-py.

The ligand 2,2',2''-(10-((6-((bis(2-(ethylthio)ethyl)amino)methyl)pyridin-2-yl)methyl)-1,4,7,10-tetraazacyclododecane-1,4,7-triyl)tris(*N*-methylacetamide) (DOTAm-py, 41 mg, 0.060 mmol) was dissolved in a CH_3OH and H_2O (1:1) mixture (20 mL) and anhydrous $TmCl_3$ (17 mg, 0.060 mmol) was added. The pH was adjusted to 7 with NaOH (aq.) and the reaction mixture was stirred at 70 °C for 72 h. The pH was monitored periodically and adjusted to 7 with NaOH (aq.) as needed. The solvent was removed under reduced pressure. The solid obtained was dissolved in water (5 mL). The solution was centrifuged to remove the unwanted solid. The solvent was removed under reduced pressure to yield the chloride salt of Tm-DOTAm-py as an off-white flaky solid (50 mg, 87%). See Figure S14 in SI for δH(500 MHz; D_2O). HR-MS found: $[M-H]^{2+}$, 424.6722. $C_{32}H_{58}N_9O_3S_2Tm^{2+}$ calc 424.6718.

Eu-DOTAm-py.

Ligand 2,2',2''-(10-((6-((bis(2-(ethylthio)ethyl)amino)methyl)pyridin-2-yl)methyl)-1,4,7,10-tetraazacyclododecane-1,4,7-triyl)tris(*N*-methylacetamide) (DOTAm-py, 11.8 mg, 0.0173 mmol), $EuCl_3{\cdot}6H_2O$ (6.3 mg, 0.017 mmol), 75 h, white powder (14 mg, 86%). See Figure S15 in SI for δH(500 MHz; D_2O). HR-MS found: $[M-H]^{2+}$, 416.6685. $C_{32}H_{58}N_9O_3S_2Eu^{2+}$ calc 416.6653.

Gd-DOTAm-py.

Ligand 2,2',2''-(10-((6-((bis(2-(ethylthio)ethyl)amino)methyl)pyridin-2-yl)methyl)-1,4,7,10-tetraazacyclododecane-1,4,7-triyl)tris(*N*-methylacetamide) (DOTAm-py, 11.8 mg, 0.0173 mmol), $GdCl_3{\cdot}6H_2O$ (6.4 mg, 0.017 mmol), 73 h, white powder (14.2 mg, 87%). HR-MS found: $[M-H]^{2+}$, 419.1701. $C_{32}H_{58}N_9O_3S_2Gd^{2+}$ calc 419.1667.

tBu-DOTAm-βAla-CBZ (4).

A solution of benzyl 1,4,7,10-tetraazacyclododecane-1-carboxylate (**3**, 114 mg, 0.370 mmol) and Cs_2CO_3 (388 mg, 1.19 mmol) in acetonitrile (50 mL) was stirred for 10 min at room temperature. Solid *tert*-butyl 3-(2-chloroacetamido)propanoate (264 mg, 1.19 mmol) was added to the reaction mixture which was further stirred at 55 °C for 36 h. The mixture was filtered, and the solvent was removed under reduced pressure. The crude solid was purified by flash chromatography over silica gel, using a gradient of 100% CH_2Cl_2 to 7% CH_3OH in CH_2Cl_2, to give the compound [**4**] as faint yellow solid (260 mg, 81%). δH(500 MHz; $CDCl_3$) 8.03 (1H, br s), 7.46-7.44 (1H, m), 7.38-7.31 (5H, m), 5.36-4.94 (2H, s), 3.69-3.41 (12H, m), 3.22-2.76 (10H, m), 2.69-2.29 (12H, m), 1.48-1.38 (27H, m). HR-MS found: $[M+H]^+$, 862.5295. $C_{43}H_{72}N_7O_{11}^+$ calc 862.5284.

tBu-DOTAm-βAla (5).

The catalyst 10% Pd/C (18 mg) was added to a solution of the tri-*tert*-butyl 3,3',3''-((2,2',2''-(10-((benzyloxy)carbonyl)-1,4,7,10-tetraazacyclododecane-1,4,7-

triyl)tris(acetyl))tris(azanediyl)tripropionate ([**4**], 180 mg, 0.209 mmol) in CH_3OH (7 mL). The mixture was shaken under an H_2 atmosphere in a Parr hydrogenator at 50 psi for 24 h. The mixture was filtered through celite. The solvent was removed under reduced pressure to afford product **5** as colorless solid that was used immediately in the next step without further purification. HR-MS found: $[M+H]^+$, 728.4919. $C_{35}H_{66}N_7O_9^+$ calc 728.4917.

tBu-DOTAm-βAla-py (6).

A solution of tri-*tert*-butyl 3,3′,3″-((2,2′,2″-(1,4,7,10-tetraazacyclododecane-1,4,7-triyl)tris(acetyl))tris(azanediyl)tripropionate (**5**, 67 mg, 0.092 mmol), Cs_2CO_3 (30 mg, 0.092 mmol) and *N*-((6-(chloromethyl)pyridin-2-yl)methyl)-2-(ethylthio)-*N*-(2-(ethylthio)ethyl)ethan-1-amine (30.6 mg, 0.092 mmol) in acetonitrile (20 mL) was stirred at 70 °C for 40 h. The mixture was filtered, and the solvent was removed under reduced pressure. The crude solid was purified by chromatography over alumina (neutral), using a gradient of 100% CH_2Cl_2 to 6% CH_3OH in CH_2Cl_2, to give the compound **6** as yellowish sticky solid (40 mg, 43%). δH(300 MHz; $CDCl_3$) 8.22 (1H, d, *J* 6.2 Hz), 7.90 (1H, br s), 7.61 (1H, t, *J* 7.4 Hz), 7.49 (1H, d, *J* 7.3 Hz), 7.33 (2H, br s), 7.16 (1H, d, *J* 8.2 Hz), 3.67-3.29 (10H, m), 3.29-2.08 (40H, m), 1.40 (27H, s), 1.30-1.07 (6H, m). δC(126 MHz; $CDCl_3$) 171.9, 171.6, 171.1, 170.9, 161.3, 156.5, 137.5, 128.6, 122.4, 80.3, 60.2, 58.9, 57.3, 57.0, 54.2, 54.1, 53.5, 53.0, 52.7, 51.7, 50.3, 47.3, 35.1, 29.5, 28.1, 26.2, 14.9. HR-MS found: $[M+H]^+$, 1024.6292. $C_{50}H_{90}N_9O_9S_2^+$ calc 1024.6297.

DOTAm-βAla-py.

Trifluoroacetic acid (TFA, 0.6 mL) was added to a stirred solution of tri-*tert*-butyl 3,3′,3″-((2,2′,2″-(10-((6-((bis(2-(ethylthio)ethyl)amino)methyl)pyridin-2-yl)methyl)-1,4,7,10-tetraazacyclododecane-1,4,7-triyl)tris(acetyl))tris(azanediyl)tripropionate (**6**, 38 mg, 0.037 mmol) in CH_2Cl_2 (1 mL) dropwise at 0 °C over 10 min. The reaction mixture was allowed to warm to room temperature and stirred at room temperature for 24 h. The reaction mixture was then concentrated under reduced pressure and was washed with CH_3OH (10 × 6 mL), with the solvent removed each time under reduced pressure to eliminate excess TFA. Complete removal of solvent gave the trifluoroacetate salt of DOTAm-βAla-py (37 mg, 70%). δH(500 MHz; CD_3OD) 9.49 (1H, br s), 9.15-8.93 (2H, m), 6.23-5.34 (12H, m), 3.58-3.48 (4H, t, *J* 9.1 Hz), 5.13-4.91 (20H, m), 4.58 (4H, t, *J* 7.0 Hz), 4.49-4.05 (10H, m), 2.98-2.73 (6H, m). δC(126 MHz; CD_3OD) 175.3, 161.9, 161.6, 158.8, 140.8, 129.7, 129.2, 118.8, 116.4, 57.9, 56.4, 54.6, 52.3, 36.6, 34.5, 26.5, 26.3, 15.0, 14.7. HR-MS found: $[M+2H]^{2+}$, 428.7247. $C_{38}H_{67}N_9O_9S_2^{2+}$ calc 428.7246.

Tm-DOTAm-βAla-py.

The ligand 3,3′,3″-((2,2′,2″-(10-((6-((bis(2-(ethylthio)ethyl)amino)methyl)pyridin-2-yl)methyl)-1,4,7,10-tetraazacyclododecane-1,4,7-triyl)tris(acetyl))tris(azanediyl))tripropionic acid (DOTAm-βAla-py, 32 mg, 0.037 mmol) was dissolved in a CH_3OH and H_2O (1:2) mixture (20 mL) and anhydrous $TmCl_3$ (10 mg, 0.037 mmol) was added. The pH was adjusted to 7 with NaOH (aq.) and the reaction mixture was stirred at 70 °C for 72 h. The pH was monitored periodically and adjusted to 7 with NaOH (aq.) as needed. The solvent was removed under reduced pressure. The solid obtained was dissolved in water (7 mL). The solution was centrifuged to remove the unwanted solid. The solvent was removed under reduced pressure to yield the thulium complex Tm-DOTAm-βAla-py as a white flaky solid (36 mg, 94%). See Figure S18 in SI for δH(500 MHz; D_2O). HR-MS found: $[M+H]^+$, 1022.3563. $C_{38}H_{63}N_9O_9S_2Tm^+$ calc 1022.3527.

Conflicts of interest

There are no conflicts of interest to declare.

Acknowledgements

This work was supported by the National Science Foundation grant no. CAREER 1151665 (V.C.P.) and by the H2020 IdentiFY projects (S.A.). G.F. was supported by FIRC (Fondazione Italiana per la Ricerca sul Cancro AIRC) fellowship. We thank Dr. Sylvie Pailloux for her assistance with NMR analysis.

Notes and references

1 K. J. Barnham and A. I. Bush, *Curr. Opin. Chem. Biol.*, 2008, **12**, 222-228.
2 K. I. Rodriguez-Castro, F.-J. Hevia-Urrutia and G. C. Sturniolo, *World J. Hepatol.*, 2015, **7**, 2859-2870.
3 M. H. Rayner and K. T. Suzuki, *Biometals*, 1994, **7**, 253-260.
4 M. A. Saghiri, A. Asatourian, J. Orangi, C. M. Sorenson and N. Sheibani, *Crit. Rev. Oncol. Hemat.*, 2015, **96**, 143-155.
5 D. W. Choi and J. Y. Koh, *Annu. Rev. Neurosci.*, 1998, **21**, 347-375.
6 C. Marchetti, *Biometals*, 2014, **27**, 1097-1113.
7 H. Gerber, F. Wu, M. Dimitrov, G. M. Garcia Osuna and P. C. Fraering, *J. Biol. Chem.*, 2017, **292**, 3751-3767.
8 N. I. Ward and J. A. Mason, *J. Radioanal. Nucl. Chem.*, 1987, **113**, 515-526.
9 M. A. Lovell, J. D. Robertson, W. J. Teesdale, J. L. Campbell and W. R. Markesbery, *J. Neurol. Sci.*, 1998, **158**, 47-52.
10 E. Gaggelli, H. Kozlowski, D. Valensin and G. Valensin, *Chem. Rev.*, 2006, **106**, 1995-2044.
11 A. I. Bush and R. E. Tanzi, *Neurotherapeutics*, 2008, **5**, 421-432.
12 L. E. Scott and C. Orvig, *Chem. Rev.*, 2009, **109**, 4885-4910.
13 A. J. M. Lubag, L. M. De Leon-Rodriguez, S. C. Burgess and A. D. Sherry, *Proc. Natl. Acad. Sci. U. S. A.*, 2011, **108**, 18400-18405.
14 L. M. De Leon-Rodriguez, A. J. M. Lubag, J. A. Lopez, G. Andreu-de-Riquer, J. C. Alvarado-Monzon and A. D. Sherry, *MedChemComm*, 2012, **3**, 480-483.
15 S. K. Ghosh, P. Kim, X.-a. Zhang, S.-H. Yun, A. Moore, S. J. Lippard and Z. Medarova, *Cancer Res.*, 2010, **70**, 6119-6127.
16 M. V. Clavijo Jordan, S.-T. Lo, S. Chen, C. Preihs, S. Chirayil, S. Zhang, P. Kapur, W.-H. Li, L. M. De Leon-Rodriguez, A. J.

M. Lubag, N. M. Rofsky and A. D. Sherry, *Proc. Natl. Acad. Sci. U. S. A.*, 2016, **113**, E5464-E5471.

17 T. Lee, X.-a. Zhang, S. Dhar, H. Faas, S. J. Lippard and A. Jasanoff, *Chem. Biol.*, 2010, **17**, 665-673.

18 V. C. Pierre, S. M. Harris and S. L. Pailloux, *Acc. Chem. Res.*, 2018, **51**, 342-351.

19 E. L. Que, E. Gianolio, S. L. Baker, A. P. Wong, S. Aime and C. J. Chang, *J. Am. Chem. Soc.*, 2009, **131**, 8527-8536.

20 E. L. Que, E. Gianolio, S. L. Baker, S. Aime and C. J. Chang, *Dalton Trans.*, 2010, **39**, 469-476.

21 E. L. Que, E. J. New and C. J. Chang, *Chem. Sci.*, 2012, **3**, 1829-1834.

22 J. H. Jang, S. Bhuniya, J. Kang, A. Yeom, K. S. Hong and J. S. Kim, *Org. Lett.*, 2013, **15**, 4702-4705.

23 Y. M. Xiao, G. Y. Zhao, X. X. Fang, Y. X. Zhao, G. H. Wang, W. Yang and J. W. Xu, *RSC Adv.*, 2014, **4**, 34421-34427.

24 W. S. Li, J. A. Luo and Z. N. Chen, *Dalton Trans.*, 2011, **40**, 484-488.

25 D. Kasala, T.-S. Lin, C.-Y. Chen, G.-C. Liu, C.-L. Kao, T.-L. Cheng and Y.-M. Wang, *Dalton Trans.*, 2011, **40**, 5018-5025.

26 X. Zhang, X. Jing, T. Liu, G. Han, H. Li and C. Duan, *Inorg. Chem.*, 2012, **51**, 2325-2331.

27 J. L. Major, G. Parigi, C. Luchinat and T. J. Meade, *Proc. Natl. Acad. Sci. U. S. A.*, 2007, **104**, 13881-13886.

28 J. L. Major, R. M. Boiteau and T. J. Meade, *Inorg. Chem.*, 2008, **47**, 10788-10795.

29 M. Regueiro-Figueroa, S. Gunduz, V. Patinec, N. K. Logothetis, D. Esteban-Gomez, R. Tripier, G. Angelovski and C. Platas-Iglesias, *Inorg. Chem.*, 2015, **54**, 10342-10350.

30 A. Mishra, N. K. Logothetis and D. Parker, *Chem. –Eur. J.*, 2011, **17**, 1529-1537.

31 K. Hanaoka, K. Kikuchi, Y. Urano and T. Nagano, *J. Chem. Soc. Perkin Trans. 2*, 2001, 1840-1843.

32 K. Hanaoka, K. Kikuchi, Y. Urano, M. Narazaki, T. Yokawa, S. Sakamoto, K. Yamaguchi and T. Nagano, *Chem. Biol.*, 2002, **9**, 1027-1032.

33 X.-a. Zhang, K. S. Lovejoy, A. Jasanoff and S. J. Lippard, *Proc. Natl. Acad. Sci. U. S. A.*, 2007, **104**, 10780-10785.

34 L. M. Matosziuk, J. H. Leibowitz, M. C. Heffern, K. W. MacRenaris, M. A. Ratner and T. J. Meade, *Inorg. Chem.*, 2013, **52**, 12250-12261.

35 C. Rivas, G. J. Stasiuk, M. Sae-Heng and N. J. Long, *Dalton Trans.*, 2015, **44**, 4976-4985.

36 J. Luo, W. S. Li, P. Xu, L. Y. Zhang and Z. N. Chen, *Inorg. Chem.*, 2012, **51**, 9508-9516.

37 Y. Q. Xu, J. Luo and Z. N. Chen, *Eur. J. Inorg. Chem.*, 2014, 3208-3215.

38 C. S. Bonnet, F. Caillé, A. Pallier, J.-F. Morfin, S. Petoud, F. Suzenet and É. Tóth, *Chem. –Eur. J.*, 2014, **20**, 10959-10969.

39 G. J. Stasiuk, F. Minuzzi, M. Sae-Heng, C. Rivas, H. P. Juretschke, L. Piemonti, P. R. Allegrini, D. Laurent, A. R. Duckworth, A. Beeby, G. A. Rutter and N. J. Long, *Chem. –Eur. J.*, 2015, **21**, 5023-5033.

40 A. C. Esqueda, J. A. Lopez, G. Andreu-De-Riquer, J. C. Alvarado-Monzon, J. Ratnakar, A. J. M. Lubag, A. D. Sherry and L. M. De Leon-Rodriguez, *J. Am. Chem. Soc.*, 2009, **131**, 11387-11391.

41 J. Yu, A. F. Martins, C. Preihs, V. C. Jordan, S. Chirayil, P. Y. Zhao, Y. K. Wu, K. Nasr, G. E. Kiefer and A. D. Sherry, *J. Am. Chem. Soc.*, 2015, **137**, 14173-14179.

42 E. D. Smolensky, M. Marjanska and V. C. Pierre, *Dalton Trans.*, 2012, **41**, 8039-8046.

43 E. A. Weitz, C. Lewandowski, E. D. Smolensky, M. Marjanska and V. C. Pierre, *ACS Nano*, 2013, **7**, 5842-5849.

44 P. C. van Zijl and N. N. Yadav, *Magn. Reson. Med.*, 2011, **65**, 927-948.

45 M. Woods, D. E. Woessner and A. D. Sherry, *Chem. Soc. Rev.*, 2006, **35**, 500-511.

46 I. Hancu, W. T. Dixon, M. Woods, E. Vinogradov, A. D. Sherry and R. E. Lenkinski, *Acta Radiol.*, 2010, **51**, 910-923.

47 D. Delli Castelli, G. Ferrauto, J. C. Cutrin, E. Terreno and S. Aime, *Magn. Reson. Med.*, 2014, **71**, 326-332.

48 D. V. Hingorani, A. S. Bernstein and M. D. Pagel, *Contrast Media Mol. Imaging*, 2015, **10**, 245-265.

49 A. Bar-Shir, N. N. Yadav, A. A. Gilad, P. C. M. van Zijl, M. T. McMahon and J. W. M. Bulte, *J. Am. Chem. Soc.*, 2015, **137**, 78-81.

50 A. Bar-Shir, A. A. Gilad, K. W. Y. Chan, G. Liu, P. C. M. van Zijl, J. W. M. Bulte and M. T. McMahon, *J. Am. Chem. Soc.*, 2013, **135**, 12164-12167.

51 R. Trokowski, J. Ren, F. K. Kálmán and A. D. Sherry, *Angew. Chem. Int. Ed.*, 2005, **44**, 6920-6923.

52 E. Kimura, S. Aoki, T. Koike and M. Shiro, *J. Am. Chem. Soc.*, 1997, **119**, 3068-3076.

53 S. Aoki, H. Kawatani, T. Goto, E. Kimura and M. Shiro, *J. Am. Chem. Soc.*, 2001, **123**, 1123-1132.

54 M. Tanaka, M. Nakamura, T. Ikeda, K. Ikeda, H. Ando, Y. Shibutani, S. Yajima and K. Kimura, *J. Org. Chem.*, 2001, **66**, 7008-7012.

55 D. M. Corsi, C. Platas-Iglesias, H. v. Bekkum and J. A. Peters, *Magn. Reson. Chem.*, 2001, **39**, 723-726.

56 O. M. Evbuomwan, G. Kiefer and A. D. Sherry, *Eur. J. Inorg. Chem.*, 2012, 2126-2134.

57 K. N. Green, S. Viswanathan, F. A. Rojas-Quijano, Z. Kovacs and A. D. Sherry, *Inorg. Chem.*, 2011, **50**, 1648-1655.

58 K. T. Barglow and B. F. Cravatt, *Angew. Chem. Int. Ed.*, 2006, **45**, 7408-7411.

59 C. F. Geraldes, A. M. Urbano, M. C. Alpoim, A. D. Sherry, K. T. Kuan, R. Rajagopalan, F. Maton and R. N. Muller, *Magn. Reson. Imaging*, 1995, **13**, 401-420.

60 S. Aime, M. Botta, G. Ermondi, F. Fedeli and F. Uggeri, *Inorg. Chem.*, 1992, **31**, 1100-1103.

61 M. Botta, *Eur. J. Inorg. Chem.*, 2000, 399-407.

62 J. H. Freed, *J. Chem. Phys.*, 1978, **68**, 4034-4037.

63 D. H. Powell, O. M. N. Dhubhghaill, D. Pubanz, L. Helm, Y. S. Lebedev, W. Schlaepfer and A. E. Merbach, *J. Am. Chem. Soc.*, 1996, **118**, 9333-9346.

64 L. Tei, Z. Baranyai, L. Gaino, A. Forgacs, A. Vagner and M. Botta, *Dalton Trans.*, 2015, **44**, 5467-5478.

65 M. Li, Y. Q. Zhang, Z. J. Liu, U. Bharadwaj, H. Wang, X. W. Wang, S. Zhang, J. P. Liuzzi, S. M. Chang, R. J. Cousins, W. E. Fisher, F. C. Brunicardi, C. D. Logsdon, C. Y. Chen and Q. Z. Yao, *Proc. Natl. Acad. Sci. U. S. A.*, 2007, **104**, 18636-18641.

66 M. Suchý, M. Milne, A. A. H. Elmehriki, N. McVicar, A. X. Li, R. Bartha and R. H. E. Hudson, *J. Med. Chem.*, 2015, **58**, 6516-6532.

67 E. L. Que and C. J. Chang, *J. Am. Chem. Soc.*, 2006, **128**, 15942-15943.

68 J. Stancanello, E. Terreno, D. D. Castelli, C. Cabella, F. Uggeri and S. Aime, *Contrast Media Mol. Imaging*, 2008, **3**, 136-149.

69 E. Terreno, J. Stancanello, D. Longo, D. D. Castelli, L. Milone, H. M. H. F. Sanders, M. B. Kok, F. Uggeri and S. Aime, *Contrast Media Mol. Imaging*, 2009, **4**, 237-247.

70 W. T. Dixon, J. Ren, A. J. M. Lubag, J. Ratnakar, E. Vinogradov, I. Hancu, R. E. Lenkinski and A. D. Sherry, *Magn. Reson. Med.*, 2010, **63**, 625-632.

71 J. W. Ponder and D. A. Case, *Adv. Protein Chem.*, 2003, **66**, 27-85.

72 B. P. Hay, *Coord. Chem. Rev.*, 1993, **126**, 177-236.

73 E. Gianolio, G. B. Giovenzana, D. Longo, I. Longo, I. Menegotto and S. Aime, *Chem. –Eur. J.*, 2007, **13**, 5785-5797.

74 S. Avedano, M. Botta, J. S. Haigh, D. L. Longo and M. Woods, *Inorg. Chem.*, 2013, **52**, 8436-8450.

75 B. P. Hay, E. J. Werner and K. N. Raymond, *Bioconjugate Chem.*, 2004, **15**, 1496-1502.

TOC: Two thulium-based paraCEST contrast agents enable detection and imaging of copper and zinc by MRI with complete on/off response.